Anisotropic galvanomagnetic effect in the quasi-two-dimensional organic conductor α-(BEDT-TTF)$_2$KHg(SCN)$_4$, where BEDT-TTF is bis(ethylenedithio)tetrathiafulvalene

T. Sasaki and N. Toyota
Institute for Materials Research, Tohoku University, Katahira 2-1-1, Aoba-ku, Sendai 980, Japan
(Received 15 November 1993)

The anisotropy of the magnetoresistance has been measured systematically by changing the current and field direction with respect to the crystallographic axes in the quasi-two-dimensional organic conductor α-(BEDT-TTF)$_2$KHg(SCN)$_4$, where BEDT-TTF denotes bis(ethylenedithio)tetrathiafulvalene, which shows an antiferromagneticlike ordering as a spin-density wave below $T_A = 10$ K. The open direction of the Fermi surface changes from $\theta = 0°$ in the normal-metal phase to 30° in the antiferromagneticlike phase (θ is the tilt angle from the c axis in the conductive a-c plane). The open direction in the normal-metal phase is in agreement with a tight-binding band-structure calculation based on the crystal structure at room temperature. Angle-dependent magnetoresistance oscillations (ADMRO's) have been measured in both phases using a double-axis sample rotation system in fields up to 26 T. In the normal-metal phase, the angle-dependent magnetoresistance oscillations show two-dimensional behavior resulting from the closed Fermi surface with cross-sectional area 14% of the Brillouin zone. On the other hand, in the antiferromagneticlike phase, the angle-dependent magnetoresistance oscillations show one-dimensional behavior, the open direction of which is along $\theta = 30°$ as observed in the current-direction dependence. At 26 T higher than H_A ($T = 1.5$ K) = 23 T, the phase boundary between the antiferromagneticlike phase and the normal-metal phase, we have observed exactly the same two-dimensional ADMRO effect as in the normal-metal phase at higher temperatures. In order to explain these anomalous temperature and field dependences of the Fermi surface, we propose a superlattice model which reconstructs the Fermi surface at the phase transition. This model shows that a pair of open Fermi surfaces in the normal-metal phase is nested to each other by the vector $\mathbf{Q}(=\frac{1}{6}\mathbf{k}_a+\frac{1}{2}\mathbf{k}_b+\frac{1}{3}\mathbf{k}_c)$ and the new open Fermi surface is reconstructed in antiferromagneticlike phase by the multiconnected closed Fermi surface.

I. INTRODUCTION

The charge-transfer organic salts (BEDT-TTF)$_2X$ constitute a family of organic conductors,[1] where X is a monovalent anion, and BEDT-TTF is bis(ethylenedithio) tetrathiafulvalene. The BEDT-TTF molecules are linked to each other by overlapping molecular π orbitals to form a two-dimensional planar conducting network. The BEDT-TTF and X layers are stacked alternately to make up the layer structure. The electronic properties show a quasi-two-dimensional nature, reflecting the crystal structure. A series of α-(BEDT-TTF)$_2M$Hg(SCN)$_4$ compounds, with $M = K$,[2] Rb,[3] NH$_4$,[4] and Tl,[5] are isostructural, with similar lattice parameters. Hereafter, we refer to these as the KHg(SCN)$_4$ salt, and so on.

The crystal structure of the KHg(SCN)$_4$ salt[2] is shown in Figs. 1(a) and 1(b). The structure is triclinic with space group $P\bar{1}$: $a = 10.082$ Å, $b = 20.565$ Å, $c = 9.933$ Å, $\alpha = 103.70°$, $\beta = 90.91°$, $\gamma = 93.06°$, and $Z = 2$ at 298 K. The projection [Fig. 1(a)] along the c direction shows a layer structure consisting of BEDT-TTF conducting layers and polymeric KHg(SCN)$_4$ anion layers. The interlayer distance is about 20 Å. Figure 1(b) shows the molecular arrangement of the BEDT-TTF's units viewed along the molecular long axis. The packing pattern is similar to that of α-(BEDT-TTF)$_2$I$_3$, which is referred to the α type.[6] According to band-structure calculations[4] based on the two-dimensional tight-binding approximation, the overlappings (-a1-b-a2-c-a1-) of the π orbitals transverse to the molecular plane are larger than the longitudinal ones (-a1-a2-a1- and -b-c-b-), because the side-by-side (sulfur-sulfur) contacts between neighboring BEDT-TTF's must be dominant to construct the two-dimensional network in the a-c plane. The anion structure is quite unusual. The thick anion layer comprises triple sheets: Hg^{2+} and M^+ ions are in the middle sheet and the linear SCN groups in the upper and lower sheets. The mercury is tetrahedrally coordinated to two sulfur

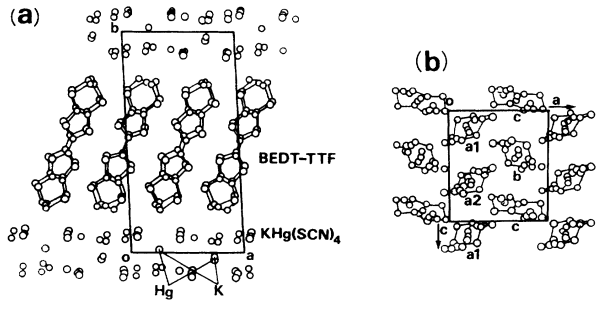

FIG. 1. (a) Crystal structure of α-(BEDT-TTF)$_2$KHg(SCN)$_4$ projected along the c direction. (b) The arrangement of BEDT-TTF molecules of positions a1, a2, b, and c in the unit cell viewed along the molecular long axis.

atoms of the two SCN groups in the upper sheet and to the other two in the bottom sheet. The M is linked with the four nitrogen atoms of the SCN groups to form a pyramid. Hence a zigzag two-dimensional network of -M-NCS-Hg-SCN- spreads over the a-c plane.

Only the $NH_4Hg(SCN)_4$ salt is known to exhibit superconductivity below about 1 K.[7] On the other hand, the $KHg(SCN)_4$ salt shows an antiferromagneticlike phase transition at $T_A \simeq 10$ K.[8] The static magnetic susceptibility χ_{spin} shows anisotropic behavior with respect to the external field direction below T_A. χ_{spin} is almost constant in a field perpendicular to the a-c plane, while it is very much less in a field parallel to the plane. Since these behaviors are indicative of antiferromagnetic (AFM) ordering with the easy axis in the a-c plane, we have proposed the possible existence of a spin-density wave (SDW) due to Fermi-surface nesting.[8] The antiferromagneticlike phase transition is associated with a shoulder-type anomaly in the zero-field electrical resistance.[9] Electron spin resonance[10] (ESR) and nuclear magnetic resonance[11] measurements also show anomalous changes, in the intensity of the ESR signal and in the proton-relaxation time below T_A, respectively. These magnetic properties have been discussed in terms of the SDW. However, the internal field expected to be caused by the SDW has not been detected so far.

The magnetoresistance (MR) below T_A shows characteristic features which were observed by Osada *et al.*[12] and have been attracting much attention. We have proposed a magnetic phase diagram based on the MR measurements.[13] Figure 2 shows (a) typical MR curves at 0.5 K in the field perpendicular to the a-c plane and (b) the resultant H-T phase diagram. The MR rapidly increases with field up to a maximum at H_C (for example, 10 T at 0.5 K). With further increase in the field the MR decreases continuously to H_A (23 T), where a kink appears and then the MR increases again. Hysteretic behavior is clearly observed for increasing and decreasing fields between H_B (7T) and H_A. Three different phases can be recognized from the temperature dependence of H_A, H_B, and H_C: a normal-metallic phase (II), a positive-MR phase (I_B), and a phase (I_A) having a negative slope of the MR accompanied by hysteresis. Hereafter, we refer to the phase II as a normal-metal phase and the phases I_A and I_B as an antiferromagneticlike phase (AFM-like phase). Similar MR behavior and a similar phase diagram have been reproduced in the $RbHg(SCN)_4$ (Ref. 14) and $TlHg(SCN)_4$ (Ref. 5) salts.

Shubnikov–de Haas (SdH) (Refs. 8 and 12–20) and de Haas–van Alphen (dHvA) (Refs. 18–20) oscillations are observed below 4 K. We have reported that the Fermi surface (FS) observed for both $H < H_A$ and $H > H_A$ is cylindrical, with the same cross-sectional area S and effective mass m^* but different Dingle temperatures T_D.[20] The observed S is in agreement with results of the band-structure calculation.[4] Figure 3 shows the FS calculated on the basis of the crystal structure at room temperature.[4] The calculation finds that two bands cross the Fermi level: one forms a two-dimensional closed orbit corresponding to the observed FS, and the other a quasi-one-dimensional open orbit (a pair of corrugated sheets). A pair of open FS's is likely to be nested with each other, leading to a possible instability against SDW formation. The origin of the antiferromagneticlike behavior mentioned above has been discussed on the basis of this instability of the quasi-one-dimensional band.[8] The effect of the antiferromagnetic ordering on the SdH and dHvA oscillations has been discussed[21] in terms of a spin-splitting effect, including the exchange interaction. Recently, we have found from Hall-resistance measurements[22] that the carrier density steeply decreases below 10 K, suggesting opening of the SDW gap on the open FS.

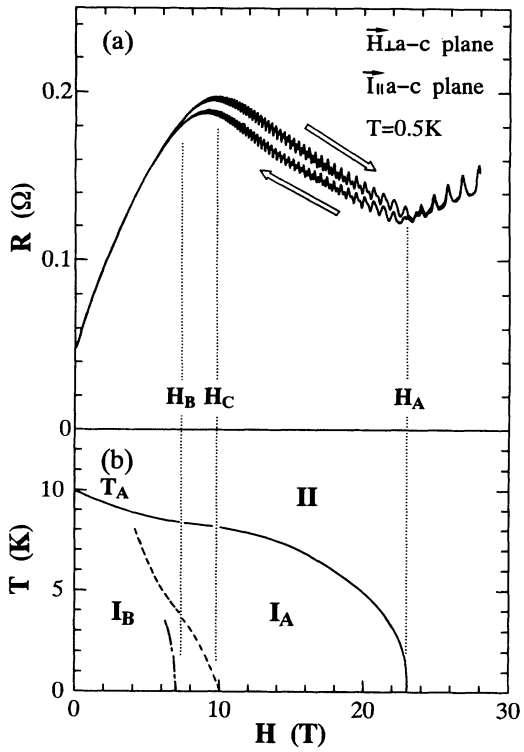

FIG. 2. (a) Magnetoresistance in the field perpendicular to the a-c plane and (b) the corresponding magnetic phase diagram. The AFM-like phase is underneath the solid line in (b).

For many BEDT-TTF salts, the effective mass m^* determined from the SdH and dHvA effects is found to be larger than the band mass m_b. This difference has been attributed to mass enhancement due to many-body renor-

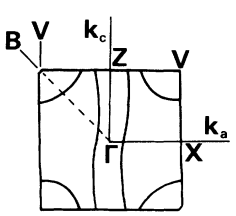

FIG. 3. Two-dimensional first Brillouin zone and FS's calculated by the tight-binding approximation in Ref. 4. There are a closed FS around the V point and a pair of open FS's along the k_c direction.

malization.[23] Singleton *et al.*[24] have reported cyclotron resonance measurements indicating a cyclotron resonance mass m_{CR} smaller by a factor of 5 than m^* on the closed orbit in the $KHg(SCN)_4$ salt. They concluded that the transport mass is enhanced mainly by electron-electron interactions, whereas m_{CR} is independent of these short-range interactions, and that electron-phonon interactions may play only a minor role in the mass enhancement. Although the carrier on the relevant open orbit is thought to be also strongly correlated, direct evidence has not been obtained yet.

In general, the galvanomagnetic effect provides valuable information about FS topology. In particular, it is useful for investigating an open FS, which cannot be detected by magnetic quantum oscillations. Recently, angle-dependent MR oscillations (ADMRO's), have been found in low-dimensional organic[25–28] and inorganic[29] conductors. The ADMRO effect is observed as MR oscillations with respect to the field direction. The oscillations are periodic in $\tan\phi$, where ϕ is the angle of the field direction to the axis perpendicular to the two-dimensional conducting plane. The period does not depend on the field strength, in contrast to the SdH effect. This effect has been explained as arising from the FS geometry, as will be described below.

The open FS predicted by the band-structure calculation is considered to play an important role in SDW and charge-density-wave CDW phase transitions. In order to study how the FS topology changes with temperature or field, the galvanomagnetic effect is measured systematically by changing the field and current direction with respect to the crystallographic axes in single crystals of the antiferromagneticlike organic conductor α-(BEDT-TTF)$_2$KHg(SCN)$_4$. In Sec. II, we describe the experimental methods for sample preparation and MR measurements. The results for the in-plane current-direction dependence of the MR and ADMRO's are presented with discussion in Secs. III A and III B, respectively. In Sec. IV, we summarize our experimental results.

II. EXPERIMENT

Single crystals of α-(BEDT-TTF)$_2$KHg(SCN)$_4$ were grown by the electro-oxidation method,[2] from a solution of BEDT-TTF in distilled 1,1,2-trichloroethane with 10 vol% ethanol, containing the purified electrolytes KSCN, $Hg(SCN)_2$, and 18-crown-6 ether. The crystals, with typical size of a few $mm^2 \times \sim 0.3$ mm, are grown on a platinum anode with a constant current of 0.5 μA. The well-developed facet is the crystallographic a-c plane. The crystal axes are determined by taking an x-ray precession photograph and measuring the anisotropy of polarized infrared reflectance spectra.[30] The electrical terminals are made of evaporated gold films, and gold wires (10-μm diameter) are glued onto the films with gold paint. The contact resistance is less than 10 Ω for each contact. Resistance measurements are done by a conventional dc method. Figures 4(a) and 4(b) show the configuration of the electrical terminals and the field direction schematically, for measurements of (a) the current-direction dependence and (b) the magnetic-field-direction dependence. In measuring the current-direction dependence, the current and voltage terminals are combined as shown in Fig. 4(a) to ensure a homogeneous current in the a-c plane. The current direction θ can be changed by selecting the combination of terminals. The field-direction dependence is studied with the current perpendicular to the a-c plane. θ and ϕ with respect to the crystallographic axes are defined as the angles rotated from the c axis in the a-c plane and from the b^* axis perpendicular to the plane, respectively. The field direction determined by θ and ϕ is changed by rotating the sample in the field with use of a double-axis rotation system combined with the 30-T hybrid magnet, or the 13-T or 15-T superconducting magnets at the High Field Laboratory for Superconducting Materials, IMR, Tohoku University. The rotation system is set in an adiabatic cell so that the temperature in a magnetic field can be controlled by a capacitance thermometer.

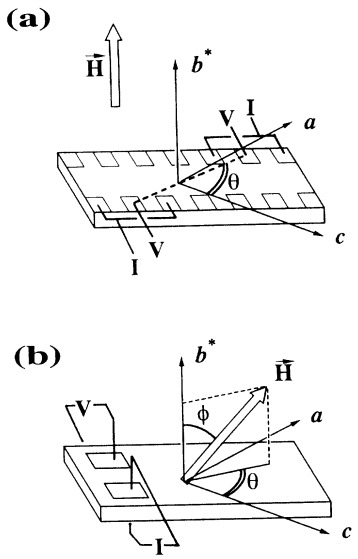

FIG. 4. Configurations of the electrical terminals, magnetic field, and crystallographic axes, and the definition of angles ϕ and θ with respect to the crystallographic axes: (a) for the current-direction and (b) for the field-direction dependence of the MR measurements.

III. RESULTS AND DISCUSSION

A. In-plane current-direction dependence of the magnetoresistance

Figure 5 shows the isothermal MR, $\Delta R/R_0 = [R(H) - R(0)]/R(0)$, as a function of the current direction θ defined in Fig. 4(a) in a constant field perpendicular to the a-c plane. The data in the upper [(i) and (f)] and lower [(b), (c), and (d)] parts of the figure were taken in the AFM-like phase and the normal-metal phase, respectively. As can be seen in the figure, the MR in each phase shows different anisotropy. In the AFM-like phase, the MR reaches a maximum around 30° and a minimum around 120°, while in the normal-metal phase, it reaches a maximum around 0° and a minimum around 90°. The solid lines are fits to the data using the function

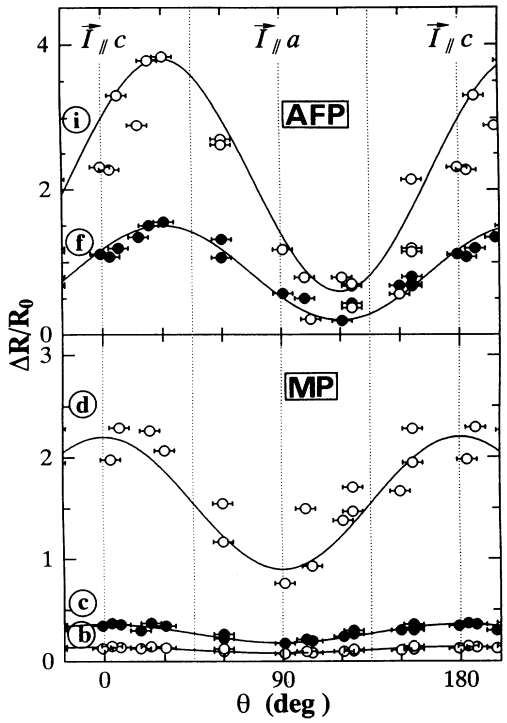

FIG. 5. Current-direction dependence of the MR in the a-c plane in a field perpendicular to the plane. The label of each set of data shows the condition of the field and temperature summarized in Table I. The data in the upper and lower figures correspond to the AFM-like phase (AFP) and the normal-metal phase (MP), respectively.

$$\frac{\Delta R}{R_0} = A + B\cos^2(\theta-\theta_0) \ . \tag{1}$$

The values of the parameters A, B, and θ_0 are listed together with the temperature and field in Table I. In both phases, the anisotropy of the MR can be well described by Eq. (1). It should be noted that the parameter θ_0, at which the MR reaches a maximum, is clearly different in the two phases: $\theta=0°$ in the normal-metal phase and $\theta=30°$ in the AFM-like phase. The histogram in Fig. 6 plots the magnitudes of A and B on the H-T phase diagram. The parameter A (hatched in the histogram), which is a constant component for the current-direction dependence, increases monotonically with increasing field

TABLE I. Parameters in Eq. (1) of the current-direction-dependent magnetoresistance.

Label	H (T)	T (K)	A	B	B/A	θ_0 (deg)
a	5.5	10.7	0.08	0.06	0.75	0
b	7.0	11.8	0.08	0.06	0.75	0
c	13.0	11.8	0.18	0.18	1.0	0
d	23.0	4.2	0.9	1.3	1.44	0
e	23.0	1.6	1.0	1.0	1.0	0
f	5.5	4.2	0.2	1.3	6.5	30
g	7.0	1.6	0.3	2.9	9.7	30
h	13.0	4.2	0.5	1.5	3.0	30
i	13.0	1.6	0.6	3.2	5.3	30

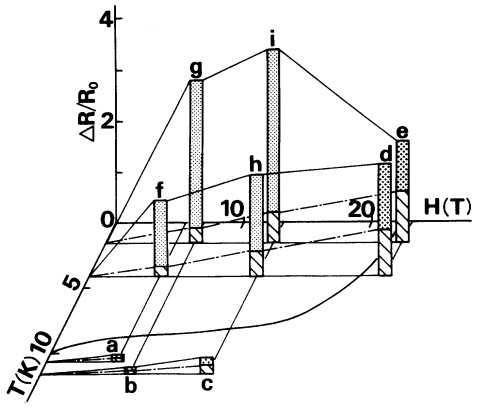

FIG. 6. Histogram of each MR component determined by Eq. (1). The hatching, shading by crosses and shading by dots correspond to the coefficients A, $B(\theta_0=0°)$, and $B(\theta_0=30°)$ in Eq. (1), respectively. The labels are the same as in Fig. 5 and Table I.

and decreasing temperature independently, on the phase boundary H_A.

The magnitude of B, $\cos^2(\theta-\theta_0)$, shows a characteristic field and temperature dependence. In the normal-metal phase, the ratio between A and B (cross shaded in the histogram) is about unity, while in the AFM-like phase B (dot shaded) is fairly large in comparison to A. These characteristic changes of both θ_0 and B are closely correlated with the phase transition between the phases.

The conductivity tensor σ_{ij} in the presence of the magnetic field can be obtained by solving the Boltzmann equation with the scattering term given by a relaxation time approximation,[31]

$$\sigma_{ij} = -\frac{e^2}{4\pi^3}\int d\mathbf{k}\frac{df_0}{d\varepsilon(\mathbf{k})}v_i(\mathbf{k},t_0) \times \int_{-\infty}^{t_0} v_j(\mathbf{k},t)\exp[(t-t_0)/\tau]dt \ , \tag{2}$$

where f_0 is the equilibrium Fermi-Dirac distribution function, τ is the relaxation time, and $v(\mathbf{k},t)$ is the momentum- and time-dependent velocity. The time dependence of the velocity is obtained from the set of equations

$$\hbar\frac{d\mathbf{k}}{dt} = -\frac{e}{c}\mathbf{v}\times\mathbf{H} \ , \tag{3}$$

$$\mathbf{v}(\mathbf{k}) = \frac{1}{\hbar}\frac{\partial\varepsilon(\mathbf{k})}{\partial\mathbf{k}} \ . \tag{4}$$

The anisotropy of σ_{ij} results from the anisotropic dispersion relation of the electron energy $\varepsilon(\mathbf{k})$, i.e., the FS topology. Ishiguro *et al.*[32] have calculated the MR using Eq. (2), based on a one-dimensional tight-binding model, in order to explain the transverse MR in the metallic region of an organic superconductor $(TMTSF)_2ClO_4$ which has an open FS only.[33] When both open and closed FS's contribute to the conduction as in the present case, the total conductivity tensor σ_{ij} can be written as the sum of each component,

$$\sigma_{ij}=\sigma_{ij}^{2D}+\sigma_{ij}^{1D} , \tag{5}$$

where σ_{ij}^{2D} and σ_{ij}^{1D} are the contributions from the closed and open FS's, respectively, and the magnetic field is applied along the z axis perpendicular to both i and j axes. The resistivity tensor ρ_{ij} can be written as

$$\rho_{xx}=\frac{\sigma_{yy}}{\sigma_{xx}\sigma_{yy}-\sigma_{xy}\sigma_{yx}} . \tag{6}$$

Taking into account the geometrical relation between the current and the open direction of the one-dimensional FS, the conductivity tensor σ_{ij}^{1D} has been calculated by Pippard.[34] The resultant MR due to the isotropic σ_{ij}^{2D} and anisotropic σ_{ij}^{1D} is described as

$$\frac{\rho_{xx}}{\rho_0}=f(H)+g(H)\cos^2\Theta , \tag{7}$$

where Θ is the angle between the current (x axis) and the open direction of a pair of open FS's, and ρ_0 is the zero-field resistivity. $f(H)$ and $g(H)$ are attributed mainly to the closed and open FS's, respectively.

Following this semiclassical treatment, it is found that the observed anisotropy of the MR with respect to the current direction could be well explained by Eq. (7); $\Theta=\theta-\theta_0$. The observation that $\theta_0=0$ in the normal-metal phase is evidence of an open FS running along the k_c direction, as expected from the band-structure calculation and shown in Fig. 3. The change of θ_0 from 0° to 30° when the system enters the AFM-like phase suggests that the topological nature of the open FS might alter, i.e., the open direction in the AFM-like phase might appear around $\theta=30°$. Hereafter, we describe the observed open FS's in the AFM-like and normal-metal phases as OFS-I and OFS-II, respectively, and the closed one as CFS.

On the basis of these results, we discuss the contributions of the CFS, OFS-I, and OFS-II to the characteristic field dependence of the MR in the AFM-like and normal-metal phases. Figure 7 schematically shows the field dependence classified into three components: the hatched part corresponds to A in Eq. (1) and Fig. 6, the dot-shaded part to B with $\theta_0=30°$, and the cross-shaded part to B with $\theta_0=0°$. Above T_A, the MR increases monotonically with field, as in a normal metal. The CFS and OFS-II contribute comparably to the MR. The characteristic MR below T_A and H_A is attributed to OFS-I. The contribution of the CFS below T_A does not change between the AFM-like and normal-metal phases. This is consistent with SdH and dHvA oscillation measurements, which show no detectable change of the cross-sectional area and the effective mass of the CFS between the two phases. The MR above H_A returns to that above T_A, indicating that OFS-I changes to OFS-II. Therefore, the characteristic MR behavior of this salt might result from OFS-I, the contribution of which depends anomalously on field.

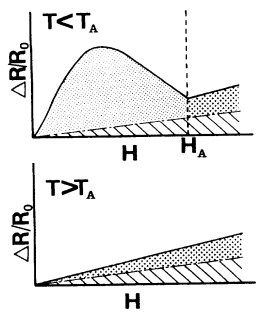

FIG. 7. Schematic MR behavior in a field perpendicular to the a-c plane at $T<T_A$ (upper figure) and $T>T_A$ (lower figure). The components hatched and shaded by crosses and dots correspond to those in Fig. 6.

As described in the Introduction, the AFM-like phase has been attributed to a SDW phase where a pair of open FS's is likely to be nested with each other. The observation of OFS-II in the normal-metal phase and the band-structure calculation might support the idea of SDW formation. If OFS-II is nested perfectly with the SDW, the open part of the FS should vanish and only the CFS at the corner of the Brillouin zone in Fig. 3 would remain. The SdH and dHvA oscillations observed in the AFM-like phase might correspond to the CFS surviving in the SDW state. However, the observation of OFS-I in the AFM-like phase suggests that the above picture for SDW formation cannot be simply applied. The question remains: what is OFS-I?

B. Angle-dependent magnetoresistance oscillation

Figure 8 shows the MR in the AFM-like phase at 1.5 K and 12.5 T as a function of the magnetic-field direction ϕ at $\theta=30°$. [See Fig. 4(b) for the configurations.] The resistance is measured along the b^* direction. The MR shows several minima at specific angles on a monotonic background, which has maxima at $\phi=0°$ and 180° and a minimum at $\phi=90°$, where the field is perpendicular and parallel to the a-c plane, respectively. The series of these local minima appears periodic in $\tan\phi$, as demonstrated in the inset. The details of the periodicity will be de-

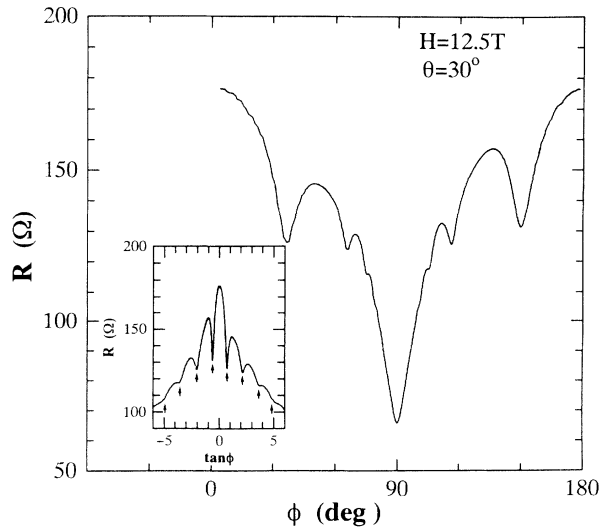

FIG. 8. Magnetic-field-direction dependence of the MR in 12.5 T at $\theta=30°$ at 1.5 K. The inset shows the $\tan\phi$ dependence of the dip position. The dips appear periodically in $\tan\phi$.

scribed below. The positions of the local minima in the AFM-like phase do not depend on the temperature and magnetic field. It is concluded that this phenomenon is different from SdH oscillations, which are visible around $\phi=0°$ and 180° (when the field is perpendicular to the plane).

Figure 9 shows the MR in a field of 12.5 T at 1.5 K as a function of the angles ϕ and θ. The period of the local minima in $\tan\phi$ becomes shortest at $\theta=30°$ and increases as θ deviates from 30°. At $\theta=30°$, the magnitude of the dips also has a maximum. In Fig. 10, the positions of the local minima are plotted in polar coordinates for $\tan\phi$ and θ. The open circles and the crosses are for two different samples. The data show that the local minima appear periodically and the period, which becomes shortest at $\theta=30°$, follows a $1/(\cos\theta)$ law. The solid lines express the periodicity, which can be described as

$$\tan\phi=\frac{1.35(n-0.45)}{\cos(\theta-30°)}\ , \tag{8}$$

where n is an integer.

The observed MR oscillations are attributed to the ADMRO effect mentioned in the Introduction, which has been reported for this salt. The early results[12,35] are not conclusive because of lack of data for double-axis rotation of the sample in the field. Recently, Iye *et al.*[36] have measured the ADMRO's in the AFM-like phase. Their measurements failed to determine the direction for the shortest period in $\tan\phi$ because their samples were twinned, with intermixed a and c axes. Kartsovnik *et al.*[37] have reported ADMRO's for the $T1Hg(SCN)_4$ salt, with almost the same parameters as in Eq. (8) in the low-temperature phase, which is considered to be the AFM-like phase, as for the $KHg(SCN)_4$ salt.

Figure 11 shows the MR and its second-derivative trace as a function of ϕ at $\theta=-95°$, at 9 K and 12.5 T in the normal-metal phase. The MR (upper curve) shows shallow minima at $\phi=0°$ and 180°, where, in the AFM-like phase, a maximum appears (Fig. 9), and a sharp minimum at $\phi=90°$. The second derivative of the MR reveals fine structure as a series of peaks marked by arrows.

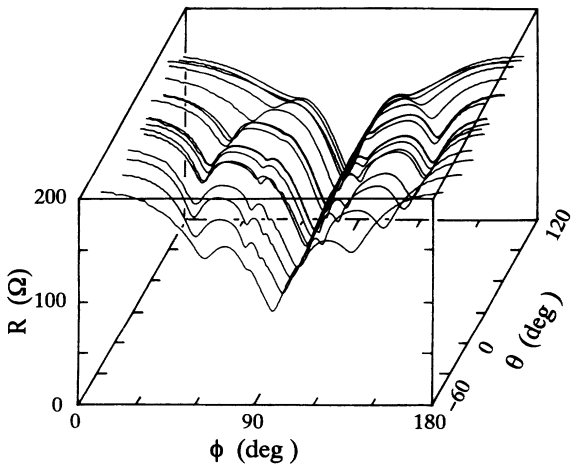

FIG. 9. Magnetoresistance as a function of the magnetic-field direction ϕ and θ in 12.5 T at 1.5 K in the AFM-like phase.

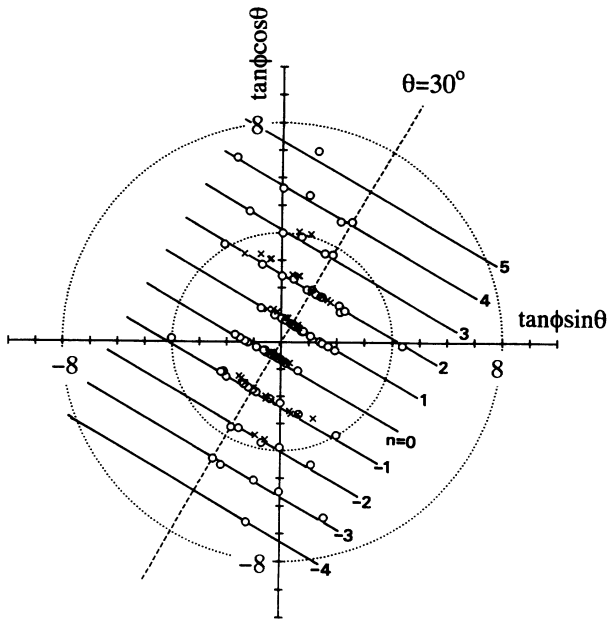

FIG. 10. Positions of the MR local minima in Fig. 9 in polar coordinates for $\tan\phi$ and θ. Circles and crosses denote different two samples. The set of solid lines numbered by n is described in Eq. (8).

Another series of peaks around $\phi=0°$ and 180° are due to the SdH effect. The peak positions indicated by arrows are periodic in $\tan\phi$, as shown in the inset. The period $\Delta(\tan\phi)$ is 1.07 at $\theta=-95°$. The θ dependence of $\Delta(\tan\phi)$ is quite different from that observed in the AFM-like phase, which will be described below. It is noted here that the phase shift appears around $\tan\phi=0$ in the plot of $\tan\phi$ vs n, as shown in the inset, while such a shift is not observed in the ADMRO's of the AFM-like phase. So far, it can be concluded that the ADMRO

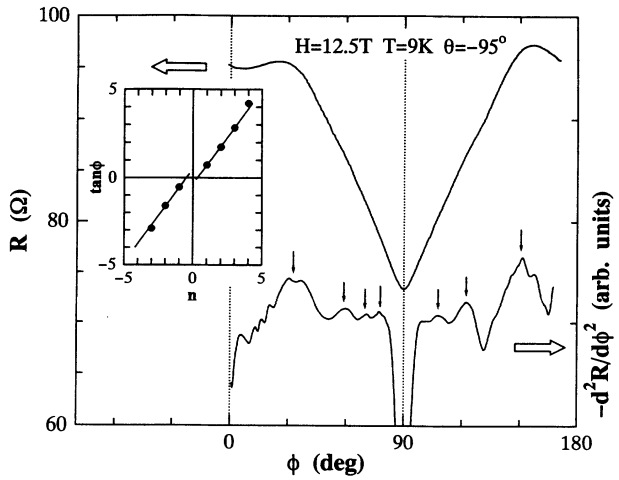

FIG. 11. Magnetic-field-direction dependence of the MR and its second-derivative curve in 12.5 T with a rotation plane of $\theta=-95°$ at 9 K in the normal-metal phase. The peaks in the second-derivative curve corresponding to the resistance fine structure are indicated by arrows. The inset shows the $\tan\phi$ dependence of the peak positions.

effect in the normal-metal phase is of a different type from that observed in the AFM-like phase.

We will briefly review the theoretical investigations of the ADMRO effect. For a quasi-two-dimensional metal having a cylindrical FS, the following model (Q2D-ADMRO) has been proposed by Yamaji.[38] The ADMRO effect is explained as arising from the geometrical properties of a weakly warped cylindrical FS. The distribution of the cross-sectional FS area cut by the planes normal to the field vanishes at certain angles. Such angles are periodic in $\tan\phi$ and satisfy

$$\tan\phi = \frac{\pi}{dk_F}(n \mp \tfrac{1}{4}) , \tag{9}$$

where $n \mp (\frac{1}{4})$ stands for $n = \pm 1, \pm 2, \pm 3, \ldots$, d is the interlayer spacing, and k_F is the radius of the cylindrical FS. An alternative explanation based on the Landau-subband dispersion has been given by Osada *et al.*[39] The energy spectrum of the Q2D system under a magnetic field is composed of a set of Landau subbands with dispersion along the field direction. The width of the Landau subbands near the Fermi level oscillates as the field direction is tilted from the normal to the two-dimensional plane. Thus the conductivity oscillates as a function of ϕ. The oscillation period satisfies the same condition as Eq. (9). On the basis of these models, Yagi *et al.*[40] have calculated the MR in the framework of semiclassical Boltzmann transport theory. The conductivity tensor is obtained for the interlayer direction as

$$\sigma_{zz} = \sigma_{zz}^0 \left[J_0^2(dk_F \tan\phi) + \sum_{n=1}^{\infty} \frac{2J_n^2(dk_F \tan\phi)}{1+(\omega_0 \tau n \cos\phi)^2} \right] , \tag{10}$$

where σ_{zz}^0 is the conductivity along the z direction in zero field, J_0 is the zeroth-order Bessel function, ω_0 is the cyclotron frequency, and τ is the relaxation time. The angles causing a minimum in σ_{zz}, corresponding to a resistance maximum, are obtained as a series of minima by varying J_0 in Eq. (10). This calculation successfully explains both the period of the ADMRO's and the resistance peaks at the angles observed in the organic conductors θ-(BEDT-TTF)$_2$I$_3$ (Ref. 25) and β-(BEDT-TTF)$_2$IBr$_2$,[26] and in the superlattice system as GaAs/Al$_x$Ga$_{1-x}$As.[29] Peschansky, Lopez, and Yao[41] have made a general analysis of the semiclassical MR of a Q2D metal in a tilted magnetic field, which confirmed the results of Yagi *et al.*[40]

For a quasi-one-dimensional (Q1D) system having a planar FS, Lebed has proposed a geometrical resonance for the electron motion in a tilted magnetic field.[42] At so-called magic angles where the electron motion becomes commensurate, it is predicted that this geometrical resonance will induce an instability of the Q1D metallic state. Although such an instability has not been established experimentally, the MR of the metallic (TMTSF)$_2$ClO$_4$ shows a series of dips at these commensurate magic angles.[27,28] Lebed and Bak[43] have calculated the MR based on an anisotropic Q2D electron spectrum. Their model shows that, at the commensurate angles, the electron scattering is enhanced due to resonance in the electron motion. Therefore resistance peaks are induced at these magic angles, which is in contradiction with the experimental result.

Recently Maki[44] and Osada, Kagoshima, and Miura[45] have calculated the MR on the basis of the Q1D energy spectrum in a tilted magnetic field. Both results show a series of the MR dips at the magic angles. The Q1D-ADMRO model proposed in Ref. 45 is briefly introduced as follows. The following Q1D band model is assumed near the Fermi level,

$$E(\mathbf{k}) = \hbar v_F(|k_x| - k_F) - \sum_{m,n} t_{mn} \cos(mbk_y + nck_z) , \tag{11}$$

where b and c are interchain distances along the y and z directions and t_{mn} ($\ll E_F$) is a transfer integral associated with the lattice vector $\mathbf{R}_{mn} = (0, mb, nc)$. The anisotropy of the transfer integrals is assumed to be $t_a > t_b \gg t_c$. When the magnetic field $\mathbf{H} = (0, H\sin\phi, H\cos\phi)$ is applied in a plane perpendicular to the one-dimensional axis, an electron near the Fermi level moves along the one-dimensional axis in real space. When the magnetic field is parallel to one of the lattice vectors $\mathbf{R}_{pq}$ (p and q are integer), electron motion on the open sheet can drift in the field direction. This drift motion carries the electric current along the field direction. For a general field direction, the electron motion hardly carries any current along the field direction because the motion is limited to the most conductive a axis. Therefore the MR shows a resonancelike dip at the magic angle ϕ_m satisfying the relation $\tan\phi_m = (pb)/(qc)$. This model has successfully explained the ADMRO's observed in (TMTSF)$_2$ClO$_4$, taking into account the triclinic structure and the anion ordering.[27,28] When the magnetic field rotates in a plane tilted by Θ from the open direction of the Q1D FS, the resonance condition is rewritten as[46]

$$\tan\phi_m \cos\Theta = \frac{pb}{qc} . \tag{12}$$

Let us now return to the ADMRO effect observed differently in the AFM-like and normal-metal phases for the KHg(SCN)$_4$ salt. First, the ADMRO effect observed in the normal-metal phase is discussed. The behavior is very similar to that in θ-(BEDT-TTF)$_2$I$_3$ and β-(BEDT-TTF)$_2$IBr$_2$, and can be explained by the Q2D-ADMRO model. Taking the θ dependence of the period of the MR peaks in $\tan\phi$ into account, the FS can be constructed by mapping the k_F obtained from Eq. (9). Figure 12 shows the cross section of the FS in the k_a-k_c plane. The open circles and crosses are for the same sample as in Fig. 10. (The filled circle was obtained above H_A at 1.5 K and will be described below.) The data points are well fit by an ellipse as shown by the solid line: $k_{Fa} = 1.65\times10^7$ cm^{-1}, $k_{Fc} = 1.05\times10^7$ cm^{-1}, and the cross-sectional area $S_{\mathrm{ADMRO}} = \pi k_{Fa} k_{Fc} = 5.4\times10^{14}$ cm^{-2}. This area is close to but slightly smaller than $S_{\mathrm{SdH}} = 6.5\times10^{14}$ cm^{-2} obtained from the SdH oscillation frequency in both phases. It is noted that S_{ADMRO} is close to $S_{\mathrm{SdH}} = 5.3\times10^{14}$ cm^{-2} observed in the NH$_4$Hg(SCN)$_4$ salt.[47] Thus we can conclude that the observed ADMRO effect in the normal-metal phase is explained by the Q2D-ADMRO model, and both the CFS and OFS-II in that phase are confirmed

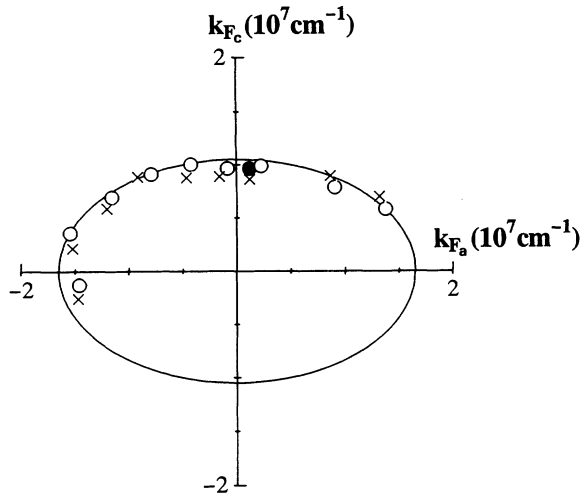

FIG. 12. Cross section of the CFS in the normal-metal phase obtained by the Q2D-ADMRO model. For explanation of the symbols, see the text.

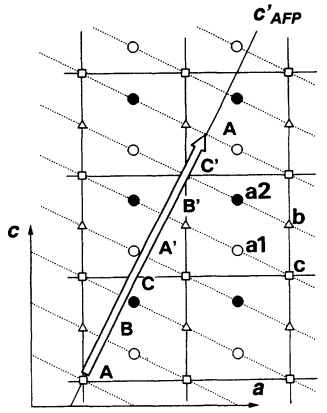

FIG. 13. Position of BEDT-TTF molecules $a1$ (circle), $a2$ (filled circle), b (triangle), and c (square) as shown in Fig. 1(b) in the a-c plane at $\frac{1}{2}b$. The large arrow indicates the proposed new lattice periodicity in the a-c plane. The dotted lines denote the BEDT-TTF chains.

to exist, in agreement with the band-structure calculation.

Secondly, we discuss the ADMRO effect in the AFM-like phase. It is difficult to explain the period $\Delta(\tan\phi)$ for the resistance dips by the Q2D-ADMRO model because $\Delta(\tan\phi)$ increases as $1/\cos(\theta-30°)$ with θ from 30°, and then k_F in Eq. (9) becomes zero at $\theta=-60°$ and 120°. Comparing the experimental result [Eq. (8)] with the model [Eq. (12)], the ADMRO effect in the AFM-like phase might be attributed to an open FS with its open direction $\theta=30°$. It is noted that the open direction of OFS-I already confirmed in Sec. III A corresponds to that observed in the ADMRO effect. Therefore, it might be concluded that the ADMRO effect in the AFM-like phase results from OFS-I. Although the electronic structure and topology of the FS in this phase are not well known, a new lattice periodicity has to be assumed to appear which changes the FS in the normal-metal phase (Fig. 3) to OFS-I and CFS in the AFM-like phase. As mentioned in Sec. III A, if simple SDW formation occurs by nesting a pair of OFS-II's only the CFS can survive in the AFM-like phase and also the Brillouin zone does not change at all. In this case, the dip position described by Eq. (12) cannot reproduce the experimental result of Eq. (8).

In order to explain the ADMRO's observed in the AFM-like phase, we propose a model of a superlattice with a reciprocal vector, the direction of which corresponds to the nesting vector for OFS-II. Thus the nesting instability induces a Peierls transition, i.e., charge-density-wave formation in this phase.

Figure 13 shows the position of BEDT-TTF molecules in the a-c plane at $\frac{1}{2}b$; the circles, filled circles, triangles, and squares denote the $a1$ $(\frac{1}{2},\frac{1}{2},\frac{1}{4})$, $a2$ $(\frac{1}{2},\frac{1}{2},\frac{3}{4})$, $b(1,\frac{1}{2},\frac{1}{2})$, and $c(1,\frac{1}{2},0)$ positions shows in Fig. 1 (b), respectively. As described in the Introduction, a band-structure calculation[4] for the normal-metal phase shown that the overlappings (-a1-b-a2-c-a1-) of the π orbitals transverse to the molecular plane are larger than the longitudinal ones (-a1-a2-a1- and -b-c-b-), and are almost equivalent for the two directions $\theta=60°$ and $-60°$. We assume that the π-orbital overlapping along $\theta=60°$ shown by the dotted lines (-a1-c-a2-b-a1-) becomes important and makes a one-dimensional conducting chain as in $(TMTSF)_2X$ salts, which is hereafter referred to a BEDT-TTF chain. The chain stacks in the a-c plane with a period of six chains (-A-B-C-A'-B'-C'-A-) along the interchain direction of $\mathbf{c}'_{AFP}=\frac{6}{5}\mathbf{a}+\frac{12}{5}\mathbf{c}$ ($c'_{AFP}\simeq 2.7\times10^{-7}$ cm and the subscript AFP refers the AFM-like phase), the direction of which corresponds to $\theta=30°$. Figure 14 shows a schematic view of the cross section for the b^*_{AFP}-c'_{AFP} plane in the AFM-like phase, which is drawn orthogonally for simplicity. Each BEDT-TTF layer consists of the BEDT-TTF chains coupled to each other. Two types of conducting layers, X and Y, stack in an antiphase [A (A'), B (B'), C (C'), A' (A), . . . , for X(Y) as shown in Fig. 14] along the b^*_{AFP} direction ($\mathbf{b}^*_{AFP}=2\mathbf{b}^*$, $b^*_{AFP}=4.0\times10^{-7}$ cm), with a period of the double layers X and Y, sandwiching the

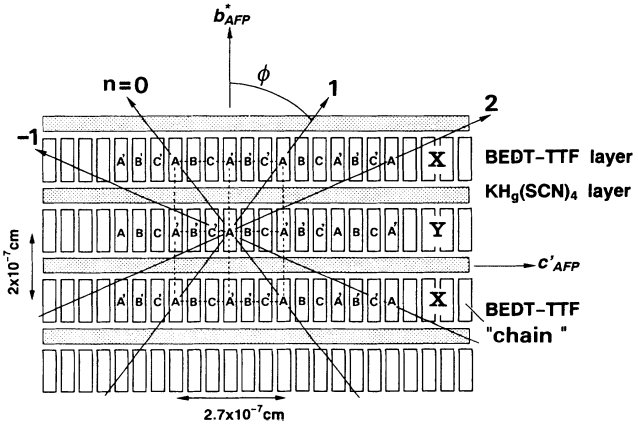

FIG. 14. Schematic cross section of the crystal in the b^*_{AFP}-c'_{AFP} plane. The BEDT-TTF layers X and Y consist of the BEDT-TTF chains. The arrows point to the field directions for the resistance dips appearing in the ADMRO's.

anionic $KHg(SCN)_4$ layer. In the Q1D-ADMRO model, a resonance causing the resistance dip occurs when the field is parallel to one of the spanning vectors, for example $-A-A-A-$, as shown by the arrows $n=0,1,2,\ldots$. These angles ϕ designated by n are described by $\tan\phi\cos(\theta-30°)=[c'_{\mathrm{AFP}}/(b^*_{\mathrm{AFP}}/2)](n-0.5)=1.35(n-0.5)$, which is consistent with the experimental result in Eq. (8). The difference of the phase factor, 0.5 versus 0.45 in Eq. (8), may result from the fact that the b^*_{AFP} direction does not coincide with the direction of $-A'-A-A'-$, because of the complicated triclinic structure.

The vector $\mathbf{Q}_{k_a-k_c}$ along the $k_{c'_{\mathrm{AFP}}}$ direction $(\frac{1}{6}\mathbf{k}_a+\frac{1}{3}\mathbf{k}_c)$, induced by the superlattice, just nests a pair of OFS-II's in the k_a-k_c plane. Therefore $\mathbf{Q}_{k_a-k_c}$ is considered to be a nesting vector which might induce a CDW instability. Figure 15 schematically shows the nesting vector $\mathbf{Q}_{k_a-k_c}$ and the FS's: the CFS (solid circles) and OFS-II (broken lines). In the present model, $\mathbf{Q}_{k_a-k_c}$ also folds the Brillouin zone, accompanied by nesting of OFS-II. The resultant CFS becomes multiconnected, as shown by the dotted circles along the $k_{c'_{\mathrm{AFP}}}$ direction. Thus an open FS is formed along the $k_{c'_{\mathrm{AFP}}}$ direction, which might correspond to OFS-I. The observed SdH oscillations in the AFM-like phase may result from the magnetic-breakdown effect on the multiconnected orbit, as pointed out by Kartsovnik, Kovalev, and Kushch.[46] In this case, the oscillation frequency is the same in both the AFM-like and the normal-metal phases which is consistent with our SdH results.[8,20] Kartsovnik and co-workers have proposed a Peierls-type transition in order to explain the ADMRO's observed in the $TlHg(SCN)_4$ salt. The present $\mathbf{Q}$ corresponds to one of the possible nesting vectors proposed for the $TlHg(SCN)_4$ salt. The FS modulated by $\mathbf{Q}$, shown in Fig. 15, results in the same topology as they proposed.

In the present model, the FS reconstructed in the AFM-like phase is expected to return to that in the normal-metal phase above H_A. Figure 16 shows ϕ dependence of the MR at $\theta=6°$ in 16 T (AFM-like) and 26 T (normal metal) at 1.5 K. In addition to the large amplitude of the SdH oscillations found in a relatively wide ϕ region centered at 0° in 26 T, the ADMRO effect is clearly observed in both fields. The ADMRO effect in 16 T well reproduces the result in Eq. (8), which is explained by the Q1D-ADMRO model with a superlattice structure, as already mentioned. However, the ADMRO effect in 26 T shows complicated features. Figure 17 plots the MR in 26 T as a function of $\tan\phi$ in order to see the ADMRO's in detail. At first sight, the oscillations do not seem to show periodicity in $\tan\phi$. It can be found, however, that the oscillations consist of two different series, which are ascribed to the Q1D- and Q2D-ADMRO's as follows. The arrows indicate the intrinsic positions of the resistance peaks arising from the Q2D-ADMRO effect on the CFS. The inset (left side) shows

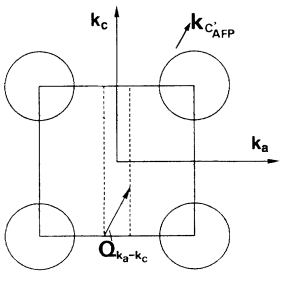

FIG. 15. Two-dimensional first Brillouin zone and the CFS (solid circle) and OFS-II (broken lines). The vector $\mathbf{Q}_{k_a-k_c}$ corresponds to a superlattice vector along the c'_{AFP} direction. The OFS-II disappears with the nesting vector $\mathbf{Q}_{k_a-k_c}$. The CFS is modified to form a multiconnected FS along the $k_{c'_{\mathrm{AFP}}}$ direction. OFS-I is induced in the AFM-like phase by the multiconnected CFS. A multiconnected FS has been proposed also in the $TlHg(SCN)_4$ salt in Ref. 46.

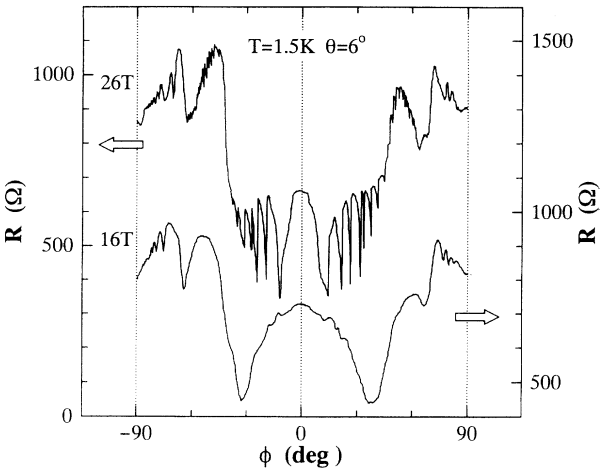

FIG. 16. Magnetoresistance traces at 1.5 K in 16 T (AFM-like phase) and 26 T (normal-metal phase) at $\theta=6°$.

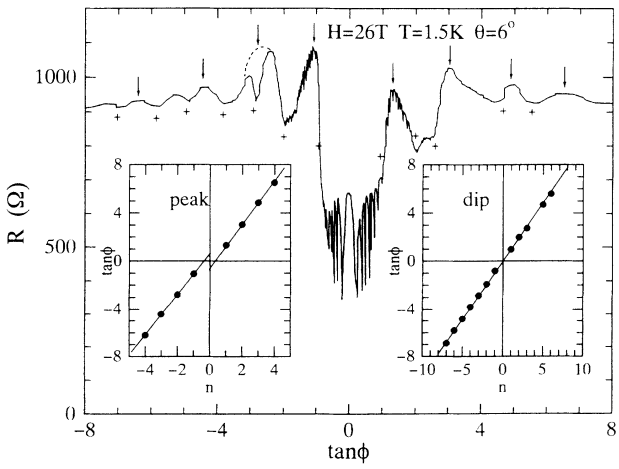

FIG. 17. The $\tan\phi$ dependence of the MR at $\theta=6°$ at 1.5 K in 26 T (normal-metal phase). The arrows and crosses show the intrinsic peaks and dips arising from Q2D-ADMRO and Q1D-ADMRO effects, respectively. The insets (left and right side) show the periodicity in $\tan\phi$ of peaks and dips, respectively.

that the peak position is periodic in $\tan\phi$ and the results well reproduce those obtained in the normal-metal phase at high temperature (9 K) and in low field (12.5 T), as shown by the filled circle in Fig. 12. The other peaks might be extrinsic, caused by the superposition of another series of dips on the peaks as follows. The dip series also appears with a different period in $\tan\phi$ from the peak series. The other inset (right side) shows the periodicity of the dips in $\tan\phi$. It is noted that the linear dependence crossing the origin at $\tan\phi=0$ and $n=0$ is similar to that presented in the original work on the Q1D-ADMRO model.[44,45] This suggests that, above H_A, the superlattice might removed. The Q1D-ADMRO's in the normal-metal phase should be due to OFS-II, although it has not been confirmed yet because of the lack of data for the θ dependence. Systematic measurements of the ADMRO effect in high fields will be necessary to get insight into the FS above H_A.

IV. SUMMARY

In this paper, we have reported on the current- and field-direction dependence of the MR in the organic conductor α-(BEDT-TTF)$_2$KHg(SCN)$_4$. We summarize here the FS topology experimentally established in the normal-metal and AFM-like phases. (i) The CFS and OFS-II running along the k_c direction exist in the normal-metal phase, just as expected from the band-structure calculation. (ii) (a) In the AFM-like phase, OFS-II disappears but a different open FS (OFS-I) appears with its open direction tilted by 30° from the k_c direction. (b) The CFS (which is not observed in the present ADMRO studies) does not change with field up to above H_A, as clarified in our SdH and dHvA measurements.[20] (iii) (a) In high field above H_A, in what has been interpreted as the normal-metal phase, the CFS determined from the Q2D-ADMRO model just coincides with that measured in the normal-metal phase at high temperatures. (b) The open direction of OFS-II is again just parallel to the k_c direction as in the normal-metal phase at high temperatures.

The difference of the FS topology between the two phases is explained by introducing a periodic potential with the reciprocal-lattice vector $\mathbf{Q}=\frac{1}{6}\mathbf{k}_a+\frac{1}{2}\mathbf{k}_b+\frac{1}{3}\mathbf{k}_c$ to the electron system, on the basis of the Q1D-ADMRO model. This lattice vector is assumed to be caused by CDW ordering via nesting of OFS-II.

We discuss here the ground state of the AFM-like phase from the two different viewpoints of SDW and CDW condensates. Both density-wave states would open a gap on OFS-II by nesting so that the carrier density would decrease below T_A, which is consistent with our Hall-effect measurements.[22] However, the anisotropic behavior of χ_{spin}, which is evidence for SDW ordering, cannot be explained by a CDW, because a CDW, in general, could induce via the Zeeman effect an isotropic decrease of the Pauli susceptibility observed above T_A. We arrive at the possibility that the ground state below T_A could be a SDW (or a CDW) accompanied by a CDW (or a SDW). In fact, it is well known that the $2k_F$ SDW induces a $4k_F$ CDW via exchange striction as observed in chromium by x-ray[48] and neutron[49,50] diffraction measurements. Diffraction measurements on our system would be valuable in order to clarify what the ground state is.

It is quite interesting to study the magnetic-field effects on the AFM-like phase, which show prominent anomalies in the magnetotransport. One of the most important results in this paper is that the FS topology above H_A is most likely to return to that in the normal-metal phase at high temperatures, strongly suggesting that the CDW might be destroyed at H_A (23 T at 1.5 K). It must be again noted, as described in the Introduction, that nonlinear field dependence of the Hall resistivity[22] appears below H_A and the differential Hall coefficient above H_A approaches that above T_A. This fact suggests that the carrier density increases monotonically with field up to H_A and becomes almost equal to that above T_A. This is consistent with field-induced suppression of the CDW at H_A. It is an open question how the magnetic field interacts with the density waves and what the mechanism is.

Recently, Singleton *et al.*[51] and Kartsovnik *et al.*[52] have reported measurements of the ADMRO effect in the KHg(SCN)$_4$ salt and proposed a different nesting vector Q in the AFM-like phase from ours. The discrepancy may be attributed to the fact that they obtained somewhat different parameters in Eq. (8) from ours.

ACKNOWLEDGMENTS

We would like to thank H. Sato, S. Endo, Dr. Y. Watanabe (IMR, Tohoku University), Dr. H. Tajima (Tokyo University), R. Tsuchiya, Professor T. Takahashi (Gakushuin University), Dr. T. Mori (IMS), Dr. H. Mori (ISTEC), Professor Y. Uemura (Columbia University), Dr. T. Osada (RCAST, Tokyo University), Dr. M. Kataoka, Dr. F. L. Pratt (IMR, Tohoku University), Professor K. Maki (USC), Dr. M. V. Kartsovnik (Kyoto University), Dr. J. Singleton (Oxford University), and Professor J. S. Brooks (Boston University) for their collaboration and discussions. Professor T. Fukase and Y. Nakagawa are appreciated for their encouragement. This work was carried out at the High Field Laboratory for Superconducting Materials, IMR, Tohoku University and partially supported by a Grant-in-Aid for Scientific Research from the Ministry of Education, Science and Culture of Japan.

[1]T. Ishiguro and K. Yamaji, *Organic Superconductors* (Springer-Verlag, Berlin, 1990).

[2]M. Oshima, H. Mori, G. Saito, and K. Oshima, Chem. Lett. **1989**, 1159 (1989).

[3]H. Mori, S. Tanaka, K. Oshima, M. Oshima, and G. Saito, Solid State Commun. **74**, 1261 (1990).

[4]H. Mori, S. Tanaka, M. Oshima, G. Saito, T. Mori, Y. Maruyama, and H. Inokuchi, Bull. Chem. Soc. Jpn. **63**, 2183 (1990).

[5]N. D. Kushch, L. I. Buravov, M. V. Kartsovnik, V. N. Laukhin, S. I. Pesotskii, R. P. Shibaeva, L. P. Rozenberg, E. B.

Yagbuskii, and A. V. Zvarikina, Synth. Met. **46**, 271 (1992).
[6]K. Bender, I. Henning, D. Schweitzer, K. Dietz, H. Endres, and H. J. Keller, Mol. Cryst. Liq. Cryst. **108**, 359 (1984).
[7]H. H. Wang, K. D. Carlson, U. Geiser, W. K. Kwok, M. D. Vashon, J. E. Thompson, N. F. Larsen, G. D. McCabe, R. S. Hulscher, and J. M. Williams, Physica C **166**, 57 (1990).
[8]T. Sasaki, H. Sato, and N. Toyota, Synth. Met. **41–43**, 2211 (1991).
[9]T. Sasaki, N. Toyota, M. Tokumoto, N. Kinoshita, and H. Anzai, Solid State Commun. **75**, 93 (1990).
[10]N. Kinoshita, M. Tokumoto, and H. Anzai, J. Phys. Soc. Jpn. **59**, 3410 (1990).
[11]T. Takahashi, R. Tsuchiya, K. Kanoda, M. Watabe, T. Sasaki, and N. Toyota, Synth. Met. **55–57**, 2513 (1993).
[12]T. Osada, R. Yagi, A. Kawasumi, S. Kagoshima, N. Miura, M. Oshima, and G. Saito, Phys. Rev. B **41**, 5428 (1990).
[13]T. Sasaki and N. Toyota, Solid State Commun. **82**, 447 (1992).
[14]J. S. Brooks, S. J. Klepper, C. C. Agosta, M. Tokumoto, N. Kinoshita, Y. Tanaka, S. Uji, H. Aoki, A. S. Perel, G. J. Athas, X. Chen, D. A. Howe, and H. Anzai, Physica B **184**, 489 (1993).
[15]T. Sasaki, N. Toyota, M. Tokumoto, N. Kinoshita, and H. Anzai, Solid State Commun. **75**, 97 (1990).
[16]M. Tokumoto, A. G. Swanson, J. S. Brooks, C. C. Agosta, S. T. Hannahs, N. Kinoshita, H. Anzai, and J. R. Anderson, J. Phys. Soc. Jpn. **59**, 2324 (1990).
[17]F. L. Pratt, J. Singleton, M. Doporto, A. J. Fisher, T. J. B. M. Janssen, J. A. A. J. Perenboom, M. Kurmoo, W. Hayes, and P. Day, Phys. Rev. B **45**, 13 904 (1992).
[18]J. S. Brooks, C. C. Agosta, S. J. Klepper, M. Tokumoto, N. Kinoshita, H. Anzai, S. Uji, H. Aoki, A. S. Perel, G. J. Athas, and D. A. Howe, Phys. Rev. Lett. **69**, 156 (1992).
[19]W. Biberacher, C. P. Heidmann, H. Müller, W. Joss, Ch. Probst, and K. Andres, Synth. Met. **55–57**, 2241 (1993).
[20]T. Sasaki and N. Toyota, Synth. Met. **55–57**, 2296 (1993).
[21]T. Sasaki and N. Toyota, Phys. Rev. B **48**, 11 457 (1993).
[22]T. Sasaki, S. Endo, and N. Toyota, Phys. Rev. B **48**, 1928 (1993).
[23]N. Toyota, E. W. Fenton, T. Sasaki, and M. Tachiki, Solid State Commun. **72**, 859 (1989).
[24]J. Singleton, F. L. Pratt, M. Doporto, T. J. B. M. Janssen, M. Kurmoo, J. A. A. J. Perenboom, W. Hayes, and P. Day, Phys. Rev. Lett. **68**, 2500 (1992).
[25]K. Kajita, Y. Nishio, T. Takahashi, W. Sasaki, R. Kato, H. Kobayashi, A. Kobayashi, and Y. Iye, Solid State Commun. **70**, 1189 (1989).
[26]M. V. Kartsovnik, V. N. Laukhin, S. I. Pesotskii, I. F. Schegolev, and V. M. Yakovenko, J. Phys. I (France) **2**, 89 (1991).
[27]T. Osada, A. Kawasumi, S. Kagoshima, N. Miura, and G. Saito, Phys. Rev. Lett. **66**, 1525 (1991).
[28]M. J. Naughton, O. H. Chung, M. Chaparala, X. Bu, and P. Coppens, Phys. Rev. Lett. **67**, 3712 (1991).
[29]R. Yagi, Y. Iye, Y. Hashimoto, T. Odagiri, H. Noguchi, H. Sakai, and T. Ikoma, J. Phys. Soc. Jpn. **60**, 3784 (1990).
[30]M. Tamura, R. Masuda, T. Naito, H. Tajima, H. Kuroda, A. Kobayashi, K. Yakushi, R. Kato, H. Kobayashi, M. Tokumota, N. Kinoshita, and H. Anzai, Synth. Met. **41–43**, 2499 (1991).
[31]R. G. Chambers, Proc. R. Soc. London, Ser. A **238**, 344 (1956).
[32]T. Ishiguro, K. Kajimura, H. Bando, K. Murata, and H. Anzai, Mol. Cryst. Liq. Cryst. **119**, 19 (1985).
[33]TMTSF is a tetramethyltetraselenafulvalene. For details, see Ref. 1.
[34]A. B. Pippard, *Magnetoresistance in Metals* (Cambridge University, Cambridge, England, 1989).
[35]T. Osada, R. Yagi, A. Kawasumi, S. Kagoshima, N. Miura, M. Oshima, H. Mori, T. Nakamura, and G. Saito, Synth. Met. **41–43**, 2171 (1991).
[36]Y. Iye, R. Yagi, N. Hanasaki, S. Kagoshima, H. Mori, H. Fujimoto, and G. Saito, J. Phys. Soc. Jpn. **63**, 674 (1994).
[37]M. V. Kartsovnik, A. E. Kovalev, V. N. Laukhin, and S. I. Pesotskii, J. Phys. I (France) **2**, 223 (1992).
[38]K. Yamaji, J. Phys. Soc. Jpn. **58**, 1520 (1989).
[39]T. Osada, R. Yagi, S. Kagoshima, N. Miura, M. Oshima, and G. Saito, in *The Physics and Chemistry of Organic Superconductors,* edited by G. Saito and S. Kagoshima, Springer Proceedings in Physics Vol. 51 (Springer-Verlag, Berlin, 1990).
[40]R. Yagi, Y. Iye, T. Osada, and S. Kagoshima, J. Phys. Soc. Jpn. **59**, 3069 (1990).
[41]V. G. Peschansky, J. A. Roldan Lopez, and Toyi Gnado Yao, J. Phys. I (France) **1**, 1469 (1991).
[42]A. G. Lebed, Pis'ma Zh. Eksp. Teor. Fiz. **43**, 137 (1986) [JETP Lett. **43**, 174 (1986)].
[43]A. G. Lebed and P. Bak, Phys. Rev. Lett. **63**, 1315 (1989).
[44]K. Maki, Phys. Rev. B **45**, 5111 (1992).
[45]T. Osada, S. Kagoshima, and N. Miura, Phys. Rev. B **46**, 1812 (1992).
[46]M. V. Kartsovnik, A. E. Kovalev, and N. D. Kushch, J. Phys. I (France) **3**, 1187 (1993).
[47]T. Osada, A. Kawasumi, R. Yagi, S. Kagoshima, N. Miura, M. Oshima, H. Mori, T. Nakamura, and G. Saito, Solid State Commun. **75**, 901 (1990).
[48]Y. Tsunoda, M. Mori, N. Kunitomi, Y. Teraoka, and J. Kanamori, Solid State Commun. **14**, 287 (1974).
[49]Y. Tsunoda, Y. Nakai, and N. Kunitomi, Solid State Commun. **16**, 443 (1975).
[50]C. F.Eagen and S. A. Werner, Solid State Commun. **16**, 1113 (1975).
[51]J. Singleton, J. Caulfield, P. T. J. Hendriks, J. A. A. J. Perenboom, M. V. Kartsovnik, A. E. Kovalev, W. Hayes, M. Kurmoo, and P. Day (unpublished).
[52]M. V. Kartsovnik, A. E. Kovalev, R. P. Shibaeva, L. P. Rozenberg, and N. D. Kushch, in *Proceedings of the 4th ISSP International Symposium on Frontiers in High Magnetic Fields, Tokyo, 1993* [Physica B (to be published)].

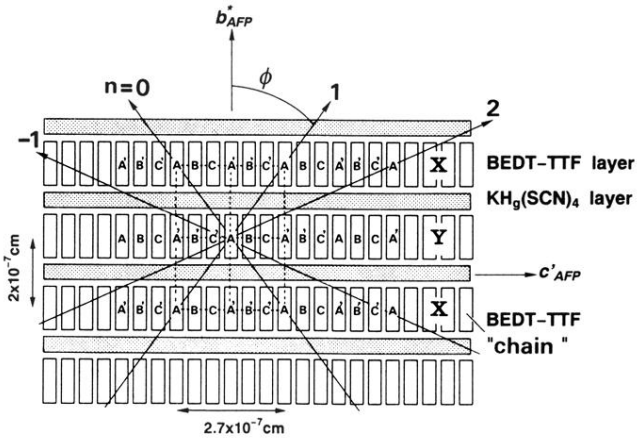

FIG. 14. Schematic cross section of the crystal in the b^*_{AFP}-c'_{AFP} plane. The BEDT-TTF layers X and Y consist of the BEDT-TTF chains. The arrows point to the field directions for the resistance dips appearing in the ADMRO's.

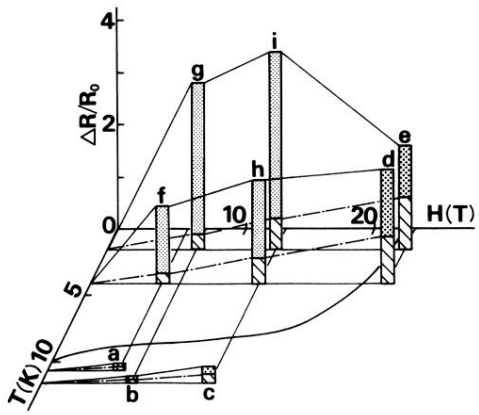

FIG. 6. Histogram of each MR component determined by Eq. (1). The hatching, shading by crosses and shading by dots correspond to the coefficients A, $B(\theta_0=0°)$, and $B(\theta_0=30°)$ in Eq. (1), respectively. The labels are the same as in Fig. 5 and Table I.

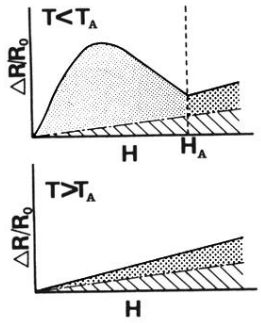

FIG. 7. Schematic MR behavior in a field perpendicular to the a-c plane at $T < T_A$ (upper figure) and $T > T_A$ (lower figure). The components hatched and shaded by crosses and dots correspond to those in Fig. 6.